COMMUNICATIONS IN NUMERICAL METHODS IN ENGINEERING
Commun. Numer. Meth. Engng 2004; **20**:845–856
Published online 9 September 2004 in Wiley InterScience (www.interscience.wiley.com). DOI: 10.1002/cnm.717

Comparison between cohesive zone models

K. Y. Volokh*,†

Faculty of Civil and Environmental Engineering, Technion, Haifa 32000, Israel

SUMMARY

Cohesive zone models (CZMs) are widely used for numerical simulation of the fracture process. Cohesive zones are surfaces of discontinuities where displacements jump. A specific constitutive law relating the displacement jumps and proper tractions defines the cohesive zone model. Within the cohesive zone approach crack nucleation, propagation, and arrest are a natural outcome of the theory. The latter is in contrast to the traditional approach of fracture mechanics where stress analysis is separated from a description of the actual process of material failure.

The common wisdom says that only cohesive strength—the maximum stress on the traction–separation curve—and the separation work—the area under the traction–separation curve—are important in setting a CZM while the shape of the traction–separation curve is subsidiary. It is shown in our note that this rule may not be correct and a specific shape of the cohesive zone model can significantly affect results of the fracture analysis. For this purpose four different cohesive zone models—bilinear, parabolic, sinusoidal, and exponential—are compared by using a block-peel test, which allows for simple analytical solutions. Numerical performance of the cohesive zone models is considered. It appears that the convergence properties of nonlinear finite element analyses are similar for all four CZMs in the case of the block-peel test. Copyright © 2004 John Wiley & Sons, Ltd.

1. INTRODUCTION

The idea to describe fracture as a material separation across a surface was pioneered by Barenblatt [1]. It appears by different names in the modern literature. We call it cohesive zone model (CZM). The cohesive zone is a surface in a bulk material where displacement discontinuities occur. Thus, continuum is enhanced with discontinuities in the form of displacement jumps. The latter requires an additional constitutive description. Equations relating normal and tangential displacement jumps across the cohesive surfaces with the proper tractions define a specific CZM. There are plenty of proposals of the 'cohesive' constitutive equations: Barenblatt [1]; Dugdale [2]; Needleman [3]; Rice and Wang [4]; Tvergaard and Hutchinson [5]; Xu and Needleman [6]; Camacho and Ortiz [7]; Geubelle and

*Correspondence to: K. Y. Volokh, Faculty of Civil and Environmental Engineering, Technion, Haifa 32000, Israel.
†E-mail: cvolokh@tx.technion.ac.il

Contract/grant sponsor: Technion

Received 29 September 2003
Accepted 14 January 2004

Baylor [8]. In accordance with the elementary functions used in CZMs they can be classified as (1) multilinear, (2) polynomial, (3) trigonometric, and (4) exponential. All these models, irrespective of the choice of the elementary functions, are constructed qualitatively as follows: tractions increase, reach a maximum, and then approach zero with increasing separation. This scenario is in harmony with our intuitive understanding of the rupture process. It is analogous to atomic interactions.

Needleman [3] introduced the cohesive zone models in computational practice. Since then CZMs are used increasingly in finite element simulations of crack tip plasticity and creep; crazing in polymers; adhesively bonded joints; interface cracks in bimaterials; delamination in composites and multilayers; fast crack propagation in polymers, and so on. Among numerous works where CZMs have been used in computer simulation we mention a few with extensive literature references: Alfano and Crisfield [9]; Chandra *et al.* [10]; Foulk *et al.* [11]; Hutchinson and Evans [12]; Mohammed and Liechti [13]; Needleman [14]; Rahulkumar *et al.* [15]; Wells *et al.* [16]. It is interesting that most researchers using CZMs consider the maximum cohesive traction—the cohesive strength—and the area under the curve representing the cohesive constitutive law—the separation work—as two main parameters characterizing the separation process. Implicitly or explicitly, the specific shape of the CZM is disregarded as subsidiary. This is surprising, in a sense, because the 'shape' of a constitutive law for the bulk material is usually carefully considered (except for the linearized elasticity, of course). It seems that Chandra *et al.* [10] compared fracture predictions by using different CZMs for the first time. Particularly, they simulated a push-out test for a titanium matrix composite reinforced by silicon carbide fibers by using bilinear and exponential CZMs. These authors discovered that the fracture predictions are different for different CZMs enjoying the same cohesive strength and separation work magnitudes. Their sophisticated computations, however, are not readily tractable and reproducible.

In this work we aim at examining the fracture predictions done by four different CZMs (Section 2) considering a block-peel test (Section 3). This test seems to be as basic as possible for the assessment of different CZMs because it allows for simple analytical solutions, which are easily verified. Moreover, this peel-test is used for the convergence analysis of the finite element procedures based on different CZMs (Section 4). In Section 5 we conclude, based on the obtained results, that the role of the shape of the CZM is essential in describing the fracture process.

2. FOUR COHESIVE ZONE MODELS

Four separation laws—CZMs—are considered in this section. These laws present relationships between surface tractions T and displacement jumps Δ across the cohesive zone. Maximum surface traction $T_{\max}$ is the cohesive strength. The corresponding displacement jump is $\Delta_{\max}$. It is convenient to introduce dimensionless parameters as follows:

$$\sigma = \frac{T}{T_{\max}} \tag{1}$$

$$\delta = \frac{\Delta}{\Delta_{\max}} \tag{2}$$

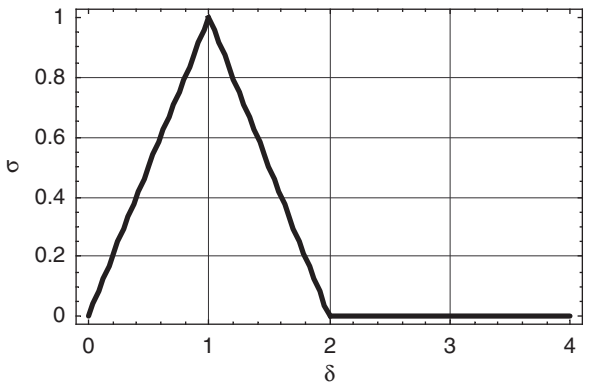

Figure 1. Bilinear CZM.

The work of separation takes the form

$$J = \int T \, \mathrm{d}\Delta \tag{3}$$

or, dimensionless

$$\phi = \frac{J}{T_{\max}\Delta_{\max}} \tag{4}$$

Bilinear CZM is shown in Figure 1. Its analytical description takes the form

$$\sigma = \begin{cases} \delta, & 0 \leqslant \delta \leqslant 1 \\ 2 - \delta, & 1 \leqslant \delta \leqslant 2 \\ 0, & 2 \leqslant \delta \end{cases} \tag{5}$$

The separation work is

$$\phi = 1 \tag{6}$$

Parabolic CZM is shown in Figure 2. Its analytical description takes the form

$$\sigma = \begin{cases} 2\delta - \delta^2, & 0 \leqslant \delta \leqslant 2 \\ 0, & 2 \leqslant \delta \end{cases} \tag{7}$$

The separation work is

$$\phi = 4/3 \cong 1.333 \tag{8}$$

Sinusoidal CZM is shown in Figure 3. Its analytical description takes the form

$$\sigma = \begin{cases} \sin(\pi\delta/2), & 0 \leqslant \delta \leqslant 2 \\ 0, & 2 \leqslant \delta \end{cases} \tag{9}$$

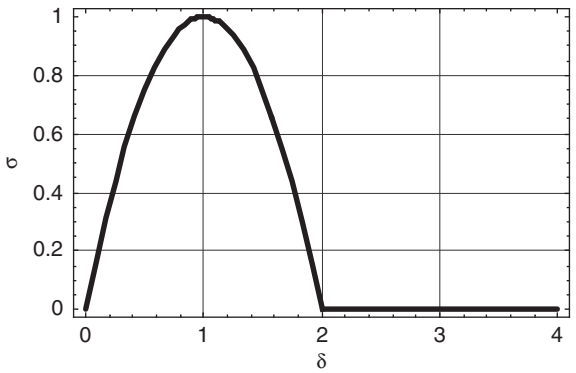

Figure 2. Parabolic CZM.

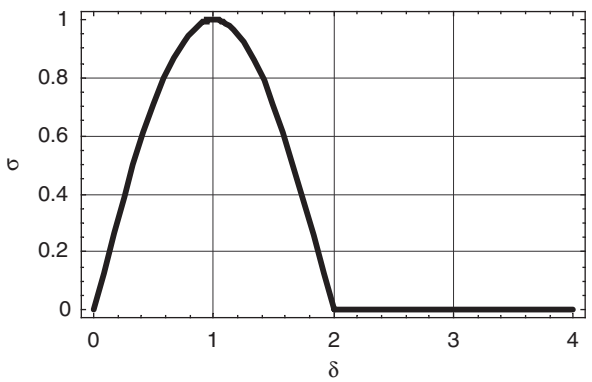

Figure 3. Sinusoidal CZM.

The separation work is

$$\phi = 4/\pi \cong 1.273 \tag{10}$$

Exponential CZM is shown in Figure 4. Its analytical description takes the form

$$\sigma = \delta \mathrm{e}^{1-\delta}, \quad 0 \leqslant \delta \tag{11}$$

The separation work is

$$\phi = e \equiv \exp(1) \cong 2.718 \tag{12}$$

It is assumed henceforth that T and Δ are tractions and displacement jumps normal to the cohesive zone. The latter is typical of Mode I opening.

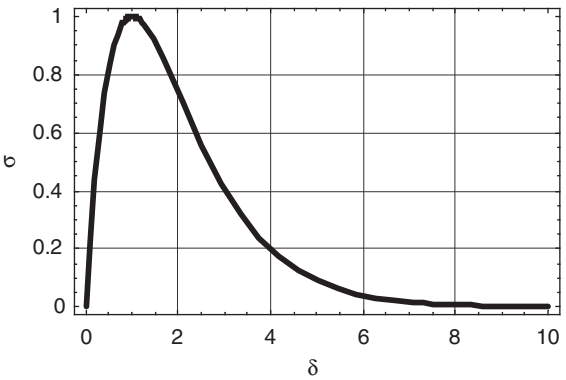

Figure 4. Exponential CZM.

3. BLOCK-PEEL TEST

Consider a body comprising two symmetric rigid parts bridged by a cohesive zone of zero thickness as shown in Figure 5. Increasing peeling forces P will lead to the nucleation of a crack at the right edge. This crack will propagate dynamically. However, it is possible to perform a quasi-static analysis of loading and to trace the equilibrium path of the structure. Since both parts of the body are rigid the only kinematical parameter is the opening angle α. The load–displacement curve P–α increases up to the critical point $(P^{\mathrm{cr}}, \alpha^{\mathrm{cr}})$. This is a limit point where equilibrium gets unstable and dynamic analysis is necessary. Crack propagation aside, P^{cr} and α^{cr} characterize the fracture process giving the maximum load, which the structure can bear, and the corresponding opening angle. These two parameters are objective in the sense that they do not depend on a specific description of the cohesive zone. The equilibrium path is described by the equation of the moment balance about the left edge of the cohesive zone

$$PL = \int_0^L Tx \, \mathrm{d}x \tag{13}$$

where L is the base length and the origin of x coordinate is at the left edge of the cohesive zone. It is convenient again to introduce dimensionless forces and generalized displacements

$$f = \frac{P}{LT_{\max}} \tag{14}$$

$$z = \frac{\alpha L}{\Delta_{\max}} \tag{15}$$

In this case Equation (13) takes the form

$$f = \frac{1}{L^2} \int_0^L \sigma(\delta) x \, \mathrm{d}x = \frac{1}{L^2} \int_0^L \sigma(\alpha x / \Delta_{\max}) x \, \mathrm{d}x = \hat{f}(z) \tag{16}$$

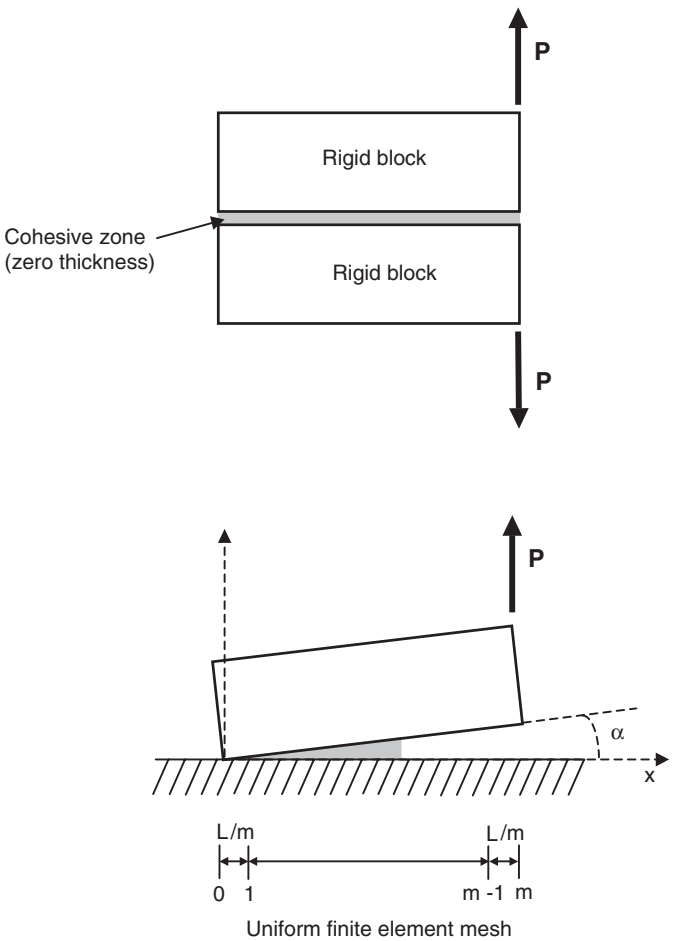

Figure 5. Block-peel test.

Substituting Equations (5), (7), (9), (11) in equation (16) we have the equilibrium equation with different cohesive zone models.
Bilinear CZM gives the following equilibrium equation:

$$\begin{aligned} f(z) &= \frac{z}{3}, \quad 0 \leqslant z \leqslant 1 \\ f(z) &= 1 - \frac{z}{3} - \frac{1}{3z^2}, \quad 1 \leqslant z \leqslant 2 \end{aligned} \tag{17}$$

It should not be missed that the bilinear CZM is on the increasing branch before point $x = L/z$ and it is on the decreasing branch after this point.

Table I. Key dimensionless parameters of different CZMs for the peel test.

CZM	Bilinear	Parabola	Sine	Exponent
ϕ	1.000	1.333	1.273	2.718
z^{cr}	1.260	1.333	1.325	1.451
f^{cr}	0.370	0.444	0.436	0.462

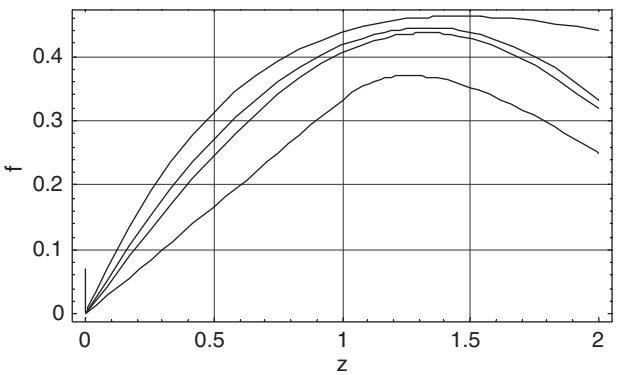

Figure 6. Exact equilibrium paths for bilinear, sinusoidal, parabolic, and exponential CZMs from the bottom to the top accordingly.

Parabolic CZM gives the following equilibrium equation:

$$f(z) = 2z/3 - z^2/4, \quad 0 \leqslant z \leqslant 2 \tag{18}$$

Sinusoidal CZM gives the following equilibrium equation:

$$f(z) = -\frac{2}{\pi z}\cos\left(\frac{\pi z}{2}\right) + \frac{4}{\pi^2 z^2}\sin\left(\frac{\pi z}{2}\right), \quad 0 \leqslant z \leqslant 2 \tag{19}$$

Exponential CZM gives the following equilibrium equation:

$$f(z) = \frac{e^{1-z}}{z^2}(-2 + 2e^z - 2z - z^2), \quad 0 \leqslant z \tag{20}$$

The interval for z is restricted by $[0, 2]$ in Equations (17)–(19) because that is enough for the subsequent analysis.

The first critical point on the equilibrium paths presented by Equations (17)–(20) is shown in Table I and in Figure 6. The second row of the table gives non-dimensional separation work ϕ; the third row of the table gives the critical opening magnitude z^{cr}; and the fourth row of the table gives the critical force magnitude f^{cr}.

Since P^{cr} and α^{cr} are objective parameters of the peel test it is possible to calibrate the CZMs by using the results shown in Table I and the following formulae

$$J = \phi\alpha^{cr}P^{cr}/(z^{cr}f^{cr}) \tag{21}$$

Table II. CZM parameters calibrated by the peel test.

CZM	Bilinear	Parabola	Sine	Exponent
J	$2.145P^{cr}\alpha^{cr}$	$2.252P^{cr}\alpha^{cr}$	$2.204P^{cr}\alpha^{cr}$	$4.054P^{cr}\alpha^{cr}$
Δ_{max}	$0.794L\alpha^{cr}$	$0.750L\alpha^{cr}$	$0.566L\alpha^{cr}$	$0.689L\alpha^{cr}$
T_{max}	$2.703P^{cr}/L$	$2.252P^{cr}/L$	$2.294P^{cr}/L$	$2.165P^{cr}/L$

$$\Delta_{max} = \alpha^{cr} L/z^{cr} \tag{22}$$

$$T_{max} = P^{cr}/(f^{cr} L) \tag{23}$$

The calibrated parameters of the CZMs are shown in Table II. It is evident from these results that the CZM parameters have to be different to correctly reproduce the peel test. It is important to emphasize that though the bulk material behaviour was highly idealized in the considered test the tendency of the result is crucial: the shape of the separation law significantly affects the fracture description.

4. NUMERICAL PERFORMANCE

From the computational point of view four considered CZMs are not equivalent. The exponential CZM is the best because it presents a smooth separation law. This is in contrast to the parabolic and sinusoidal CZMs including one vertex point at $\delta = 2$ (see Figures 2 and 3). The 'simplest' bilinear CZM is least attractive because it includes two vertex points at $\delta = 1$ and $\delta = 2$ (Figure 1). A numerical treatment of the vertex points, which correspond to inequality constraints, requires a special effort. The latter can be far from trivial. Because of the attractiveness of the exponential CZM it is of interest to compare the convergence properties of the finite element discretizations of different CZMs.

Assume that displacement jumps Δ are approximated by linear finite elements within the uniform mesh of m elements along the cohesive zone. Substituting this approximation in equilibrium equation (16) and integrating on the right hand side of it by using one-point Gauss scheme we get the following discrete formulae:

$$f_m = \frac{1}{L^2} \sum_{i=1}^{m} x_i \sigma(\delta_i) L/m \tag{24}$$

$$\delta_i = \frac{\Delta_i}{\Delta_{max}} = \frac{\alpha x_i}{\Delta_{max}} \tag{25}$$

$$x_i = \frac{L}{m}\left(i - \frac{1}{2}\right) \tag{26}$$

Substituting Equations (25) and (26) in Equation (24) we have

$$f_m = \frac{1}{m^2} \sum_{i=1}^{m} (i - 1/2)\sigma(z(i - 1/2)/m) \tag{27}$$

Using different CZMs we get corresponding discrete equations.

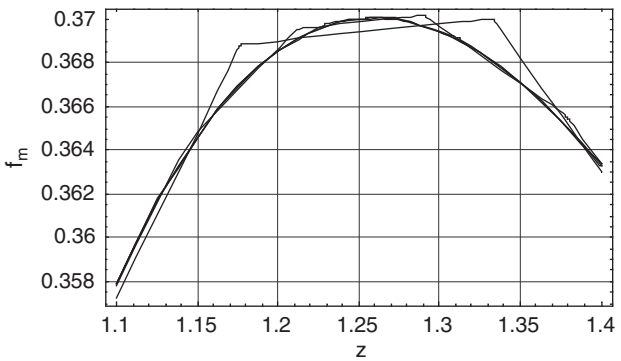

Figure 7. Equilibrium paths for bilinear CZM: 10, 20, 40, 80 and ∞ elements from the top to the bottom.

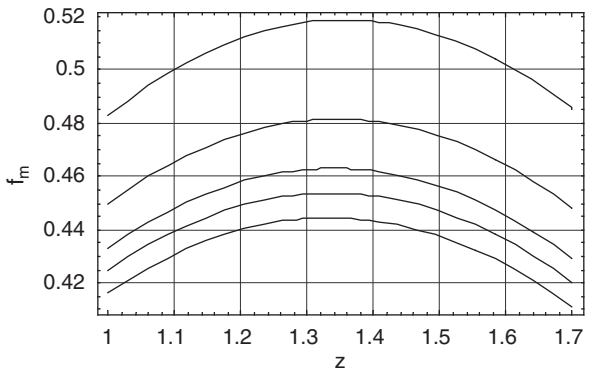

Figure 8. Equilibrium paths for parabolic CZM: 10, 20, 40, 80 and ∞ elements from the top to the bottom.

Bilinear CZM is obtained by substituting from Equation (5) in Equation (27):

$$f_m = \frac{z}{m^3}\sum_{i=1}^{n}(i-1/2)^2 + \frac{1}{m^2}\sum_{i=n+1}^{m}(i-1/2)(2-z(i-1/2)/m) \tag{28}$$

where the nth finite element is the integer closest to m/z. The graph of this equation is shown in Figure 7 for $m = 10, 20, 40, 80, \infty$ elements.

Parabolic CZM is obtained by substituting from Equation (7) in Equation (27):

$$f_m = \frac{1}{m^2}\sum_{i=1}^{m}\left(i-\frac{1}{2}\right)\left\{2\frac{z}{m}\left(i-\frac{1}{2}\right) - \frac{z^2}{m^2}\left(i-\frac{1}{2}\right)^2\right\} \tag{29}$$

Its graph is shown in Figure 8 for $m = 10, 20, 40, 80, \infty$ elements. Computations were carried out in the vicinity of the critical point only.

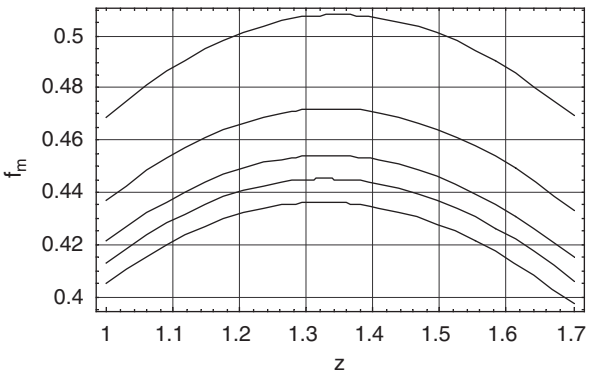

Figure 9. Equilibrium paths for sinusoidal CZM: 10, 20, 40, 80 and ∞ elements from the top to the bottom.

Sinusoidal CZM is obtained by substituting from Equation (9) in Equation (27):

$$f_m = \frac{1}{m^2}\sum_{i=1}^{m}\left(i-\frac{1}{2}\right)\sin\left\{\frac{z\pi}{2m}\left(i-\frac{1}{2}\right)\right\} \tag{30}$$

Its graph is shown in Figure 9 for $m = 10, 20, 40, 80, \infty$ elements. Computations were carried out in the vicinity of the critical point only.

Exponential CZM is obtained by substituting from Equation (11) in Equation (27):

$$f_m = \frac{z}{m^3}\sum_{i=1}^{m}\left(i-\frac{1}{2}\right)^2\exp\left\{1-\frac{z}{m}\left(i-\frac{1}{2}\right)\right\} \tag{31}$$

Its graph is shown in Figure 10 for $m = 10, 20, 40, 80, \infty$ elements. Computations were carried out in the vicinity of the critical point only.

It can be seen from Figures (7)–(10) that the convergence rate is similar for all CZMs. Consequently, the exponential CZM is still the most attractive because of its smoothness.

5. DISCUSSION

Bilinear, parabolic, sinusoidal, and exponential cohesive zone models have been compared both qualitatively and quantitatively by using the block-peel test in the present work. The results of the comparison suggest that a specific shape of the cohesive zone model can essentially affect numerical simulation of the fracture process. Moreover, the simple equating of the cohesive strength and separation work values for different CZMs is not enough in order to simulate the same fracture process. This is in contrast to the widely accepted point of view that only the cohesive strength and separation work are crucial for the cohesive zone model, while the shape of the model is subsidiary.

The results presented in our work have been obtained for an ideal rigid bulk material. Such model is chosen because it allows for the analytical consideration. This model can be directly used for analysis of building blocks in construction bridged by compliant adhesion layers. It

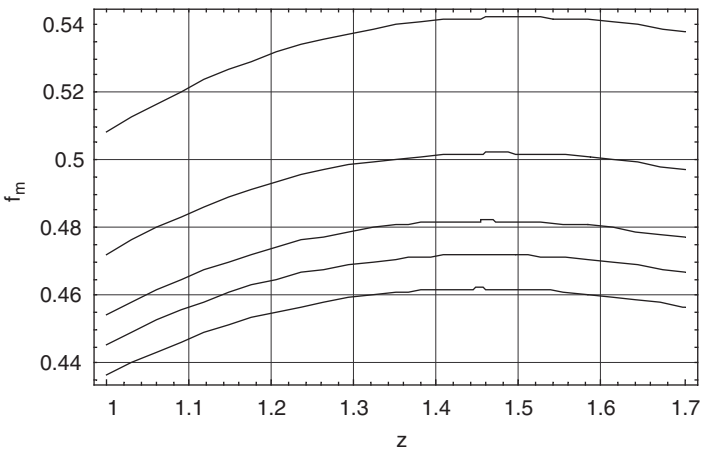

Figure 10. Equilibrium paths for exponential CZM: 10, 20, 40, 80 and ∞ elements from the top to the bottom.

is not directly applicable to modeling materials where the bulk is compliant as compared to the rigidity of the cohesive layer. However, the rigid bulk model can be accepted as a first and rough approximation to the displacement jumps field near the crack tip. Indeed, this is actually the linear approximation of the field. Thus the obtained results can be interpreted as acceptable for the compliant bulk in the asymptotic sense.

Recent numerical simulations of the push-out test for a composite material by Chandra *et al.* [10] confirm the CZM shape-sensitivity for an elastic–plastic compliant body. In principle, it is necessary to proceed with numerical testing of different CZMs for realistic material models. The problem, however, is that numerical computations can be hardly traced or reproduced independently. Besides, numerical difficulties, inherent in this type of problem, can affect the final results. These are the reasons why simple analytical models are most desirable even though the simplicity is reached at the expense of rough approximations.

Finally, it is worth emphasizing again that the main result of our work is a counterexample to the tacitly accepted rule that only cohesive strength and the separation work are important in setting a CZM while the shape of the traction–separation curve is subsidiary. This counterexample does not mean that CZMs with different shapes will always behave differently in fracture simulation. We aimed at attracting the readers' attention to the fact that the specific shape of the cohesive zone model can be very important.

ACKNOWLEDGEMENTS

This work was supported by the Fund for the Promotion of Research at the Technion.

REFERENCES

1. Barenblatt GI. The formation of equilibrium cracks during brittle fracture. General ideas and hypotheses: axially-symmetric cracks. *Journal of Applied Mathematics and Mechanics* (PMM) 1959; **23**:434–444.
2. Dugdale DS. Yielding of steel sheets containing slits. *Journal of the Mechanics and Physics of Solids* 1960; **8**:100–104.

3. Needleman A. A continuum model for void nucleation by inclusion debonding. *Journal of Applied Mechanics* 1987; **54**:525–531.
4. Rice JR, Wang J-S. Embrittlement of interfaces by solute segregation. *Material Science and Engineering A* 1989; **107**:23–40.
5. Tvergaard V, Hutchinson JW. The relation between crack growth resistance and fracture process parameters in elastic-plastic solids. *Journal of the Mechanics and Physics of Solids* 1992; **40**:1377–1397.
6. Xu XP, Needleman A. Numerical simulation of fast crack growth in brittle solids. *Journal of the Mechanics and Physics of Solids* 1994; **42**:1397–1434.
7. Camacho GT, Ortiz M. Computational modeling of impact damage in brittle materials. *International Journal of Solids and Structures* 1996; **33**:2899–2938.
8. Geubelle PH, Baylor J. Impact-induced delamination of laminated composites: a 2D simulation. *Composites Part B Engineering* 1998; **29**:589–602.
9. Alfano G, Crisfield MA. Finite element interface models for the delamination analysis of laminated composites: mechanical and computational issues. *International Journal for Numerical Methods in Engineering* 2001; **50**:1701–1736.
10. Chandra N, Li H, Shet C, Ghonem H. Some issues in the application of cohesive zone models for metal-ceramic interfaces. *International Journal of Solids and Structures* 2002; **39**:2827–2855.
11. Foulk JW, Allen DH, Helms KLE. Formulation of a three-dimensional cohesive zone model for application to a finite element algorithm. *Computer Methods in Applied Mechanics and Engineering* 2000; **183**:51–66.
12. Hutchinson JW, Evans AG. Mechanics of materials: top-down approaches to fracture. *Acta Materialia* 2000; **48**:125–135.
13. Mohammed I, Leichti KM. Cohesive zone modeling of crack nucleation at bimaterial corners. *Journal of the Mechanics and Physics of Solids* 2000; **48**:735–764.
14. Needleman A. Numerical modeling of crack growth under dynamic loading conditions. *Computational Mechanics* 1997; **19**:463–469.
15. Rahulkumar P, Jagota A, Bennison SJ, Saigal S. Cohesive element modeling of viscoelastic fracture: application to peel testing of polymers. *International Journal of Solids and Structures* 2000; **37**:1873–1897.
16. Wells GN, de Borst R, Sluys LJ. A consistent geometrically non-linear approach for delamination. *International Journal for Numerical Methods in Engineering* 2002; **54**:1333–1355.

